ATMOSPHERIC SCIENCE

Ozone depletion due to dust release of iodine in the free troposphere

Theodore K. Koenig[1,2]†, Rainer Volkamer[1,2]*, Eric C. Apel[3], James F. Bresch[4], Carlos A. Cuevas[5], Barbara Dix[1,2], Edwin W. Eloranta[6], Rafael P. Fernandez[7], Samuel R. Hall[3], Rebecca S. Hornbrook[3], R. Bradley Pierce[8], J. Michael Reeves[9], Alfonso Saiz-Lopez[5], Kirk Ullmann[3]

Iodine is an atmospheric trace element emitted from oceans that efficiently destroys ozone (O_3). Low O_3 in airborne dust layers is frequently observed but poorly understood. We show that dust is a source of gas-phase iodine, indicated by aircraft observations of iodine monoxide (IO) radicals inside lofted dust layers from the Atacama and Sechura Deserts that are up to a factor of 10 enhanced over background. Gas-phase iodine photochemistry, commensurate with observed IO, is needed to explain the low O_3 inside these dust layers (below 15 ppbv; up to 75% depleted). The added dust iodine can explain decreases in O_3 of 8% regionally and affects surface air quality. Our data suggest that iodate reduction to form volatile iodine species is a missing process in the geochemical iodine cycle and presents an unrecognized aeolian source of iodine. Atmospheric iodine has tripled since 1950 and affects ozone layer recovery and particle formation.

INTRODUCTION

Iodine is a critical micronutrient for human health transported through, and possibly partially acquired from, the atmosphere (*1*, *2*). Atmospheric iodine is prevalent in the marine boundary layer (MBL) (*3*), lower free troposphere (*4*), upper free troposphere (*5*), and stratosphere (*6*) and participates in rapid photochemical cycles, which destroy ozone (O_3) and modify the atmospheric oxidative capacity (*3*, *7–9*). Iodine photochemistry decreases the tropospheric O_3 burden by 9% (*8*, *9*), decreasing radiative forcing (*10*, *11*), and reduces the atmospheric OH burden, increasing the lifetime of methane and other greenhouse gases (*12*). On a per-atom basis, iodine is about three orders of magnitude more efficient than chlorine at destroying O_3 (*6*). Iodine oxoacids nucleate particles more efficiently than sulfuric acid (*13*), and can dominate new particle formation (NPF) and particle growth in coastal areas with macroalgae (*14*, *15*) and in the Arctic (*16*).

The global source of iodine is dominated by O_3-stimulated emissions of volatile inorganic iodine species [i.e., hypoiodous acid (HOI) and I_2] from the ocean surface (~1.86 Tg year^{-1}) (*8*, *17*, *18*). Since 1950, anthropogenic O_3 has increased the northern hemisphere iodine burden threefold over preindustrial levels via this stimulated emission (*19–21*). The oceans also dominate the atmospheric sources of organic iodine compounds, primarily methyl iodide (CH_3I), via biotic and abiotic processes (*22–24*). Biogenic sources of iodine—both

marine and terrestrial—arise from iodine's role as a micronutrient (*2*, *25*). Terrestrial iodocarbon sources are much smaller than marine sources (~0.091 Tg year^{-1}) (*22*, *26*). However, terrestrial inorganic sources of iodine originated from arid regions have not been previously considered.

Dust layers are often depleted in O_3 (*27–29*), but the necessary O_3 sink within dust plumes remains poorly understood. Previous studies have attributed dust-related O_3 loss to heterogeneous loss of O_3 and NO_y species on the dust surfaces. However, laboratory studies have now firmly established that the reactive uptake of O_3 is low (reactive uptake coefficient, $\gamma_{O3} \leq 6.6 \times 10^{-7}$) (*30*), leaving most of the necessary O_3 sink associated with dust unexplained. Previous field measurements have also found large enhancements in gas-phase iodine, both iodine monoxide (IO) and CH_3I, associated with dust layers from the Sahara (*31*, *32*). However, a possible role of iodine in the O_3 depletion has not been previously assessed, nor has an aeolian iodine source to the atmosphere been established.

RESULTS

Decoupled layers enriched in iodine and dust

During aircraft flights out of Antofagasta, Chile, in the southern hemisphere tropics, we have consistently detected widespread elevated layers of dust containing enhanced mixing ratios of IO radicals. These layers were detected on the top of the MBL and extended several kilometers into the lower free troposphere (1.5- to 7-km altitude). The dust layers were tracked by the High Spectral Resolution Lidar (HSRL) above and below the Gulfstream V (GV) aircraft (Fig. 1, A and B) to extend from 35.0°S to 12.6°S and up to 455 km from shore and persisted for the entire period (13 days) of aircraft observation. The Airborne Multi-Axis Differential Optical Absorption Spectroscopy (AMAX-DOAS) instrument found IO enhancements for all 27 layer intercepts when clouds did not preclude observation (table S1). This included multiple intercepts of likely contiguous layers along and away from the coast, indicating that IO enhancements are a persistent feature of these layers (fig. S1).

Figure 1C shows spectral proof of IO fingerprint absorption, and its variation with altitude during one of these dust intercept vertical

[1]Department of Chemistry, University of Colorado Boulder, Boulder, CO, USA. [2]Cooperative Institute for Research in Environmental Sciences, Boulder, CO, USA. [3]Atmospheric Chemistry Observations & Modeling Laboratory, National Center for Atmospheric Research, Boulder, CO, USA. [4]Mesoscale & Microscale Meteorology Laboratory, National Center for Atmospheric Research, Boulder, CO, USA. [5]Department of Atmospheric Chemistry and Climate, Institute of Physical Chemistry Rocasolano, Spanish National Research Council (CSIC), Madrid, Spain. [6]Space Science and Engineering Center, University of Wisconsin, Madison, WI, USA. [7]Institute for Interdisciplinary Science, National Research Council (ICB-CONICET), FCEN-UNCuyo, Mendoza, Argentina. [8]The National Environmental Satellite, Data, and Information Service (NESDIS), Madison, WI, USA. [9]Earth Observing Laboratory, National Center for Atmospheric Research, Boulder, CO, USA.
*Corresponding author. Email: rainer.volkamer@colorado.edu
†Present address: State Key Joint Laboratory of Environmental Simulation and Pollution Control, College of Environmental Sciences and Engineering, Peking University, Beijing, China.
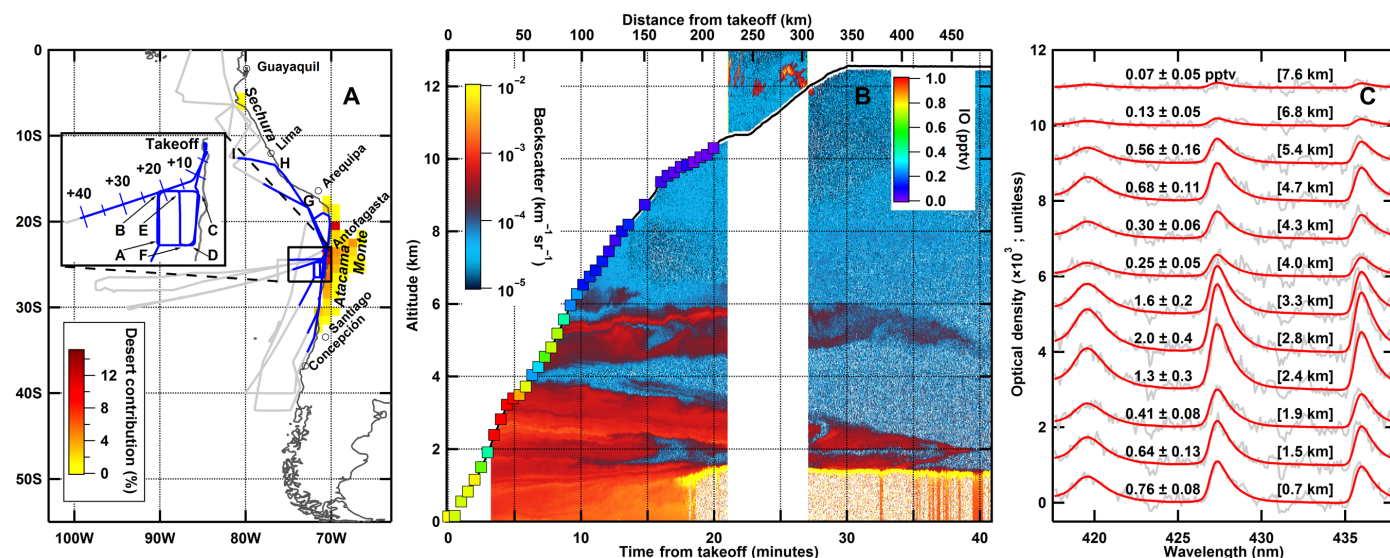
Fig. 1. Overview of observations. (A) Sources and extent of observed layers. Flight tracks for TORERO RF01 to RF06 are shown in blue where layers are contiguous with observations of enhanced IO and/or HSRL linear depolarization shows that layers below 6 km are significantly nonspherical (indicates dust); otherwise they are shown in gray. Letter labels indicate heading changes and connect with fig. S1. The background shading (yellow to red) represents the sources of observed dust based on 72-hour back-trajectories (see the Supplementary Materials for details). **(B)** DOAS and HSRL data for the takeoff of RF05 (RF05-01); the time from takeoff connects with the inset in (A). **(C)** IO spectral proofs from the case study shown in the center panel. Individual spectral proofs are vertically displaced by 1×10^{-3} in optical density for separation; numbers on the left indicate the retrieved IO mixing ratio with 1σ uncertainties, and those on the right in square brackets indicate the altitude of the observation.

profiles. The signals inside the lofted dust layers exceed those found in the MBL. The observed IO mixing ratios above, below, and between the dust layers are lower and found consistent with regional free tropospheric background of 0.10- to 0.25-pptv (parts per trillion by volume) IO (*33*). Within the dust layers, the observed IO is as much as a factor of 10 higher than this background. DOAS observations of oxygen-oxygen collision-induced observation (O_4; a reliable atmospheric standard) indicate that the dust layers reduce path length in aggregate rather than enhance it by multiple scattering, establishing unambiguously that IO concentrations are enhanced in the dust layers (fig. S2; see the Supplementary Materials for details). The IO enhancements are consistently observed in dust layers at low and high altitudes.

Back-trajectories initiated along the flight track show no contact with the MBL over up to 10 days and instead point to a terrestrial source from the Atacama, Monte, and Sechura Deserts. These deserts are portions of the South American Arid Diagonal (SAAD) (*34*). Figure 1A shows that the Atacama is the dominant source region for the intercepted layers (at least partially a reflection of proximity to most flight tracks). However, data from three layer intercepts near Peru are unambiguously from the Sechura Desert and not from the Atacama. The Atacama is the site of a globally unique extraction of iodine from caliche deposits (*35*). However, these deposits are located below the surface. Furthermore, while ore-processing facilities are located in the vicinity of many back-trajectories (i.e., located near Antofagasta where the aircraft was based), most of the back-trajectories from dust layers do not pass within 0.5° latitude or longitude of these facilities and many travel well above the boundary layer. We conclude that dust and iodine arise from a common source, i.e., the various deserts spanning the SAAD.

Ozone depletion due to iodine in the free troposphere
The lofted dust layers are consistently accompanied by significant O_3 depletion. Figure 2 shows an example of these ozone-depleted

laminae in the free troposphere. Potential temperature and humidity discontinuities at the layers' edges indicate that the vertical extent of the layers is dynamically controlled. As noted above, the layers extend horizontally over hundreds of kilometers with average O_3 depletion of 17% but as much as 40% (table S1). Near the layers' cores, O_3 drops exceptionally low [$O_3 \leq 10$ parts per billion by volume (ppbv) for 9 of 22 layers with O_3 measurements; table S1], creating ozone-depleted laminae. Aerosol counters show distinct submicrometer and supermicrometer aerosol populations in all three layers (even above 5 km; fig. S3), with the larger aerosol gravitationally settling within each layer, as indicated by the mean aerosol diameters (Fig. 2, middle). HSRL depolarization data (fig. S1) show that layers below ~5 km are nonspherical dust but become spherical at high altitude and with increasing distance from the coast (see the Supplementary Materials for details). Across all three layers, the degree of O_3 depletion correlates with aerosol surface area, consistent with the hypothesis of heterogeneous O_3 uptake—however, so does the IO mixing ratio (Fig. 2, right).

Recent laboratory studies have established that O_3 reactive uptake onto dust proceeds too slowly under atmospheric pressure to contribute substantially to O_3 loss (*30*) due to most O_3 regenerating when O_2 is present (see the Supplementary Materials for details). Heterogeneous uptake of NO_y also contributes to O_3 destruction. However, as highlighted by DOAS NO_2 measurements (fig. S2), the observed layers exist in a low NO_y environment, which limits the potential impact of heterogeneous NO_y uptake in this study. We examined the capacity for heterogeneous uptake to cause the observed O_3 depletion in the laminae, confirming a negligible impact from direct O_3 uptake and modest impacts ($\Delta O_3 \sim 10$ ppbv after 7 days) from reactive NO_y uptake (fig. S4). Heterogeneous uptake of NO_y is important but has two major limitations: (i) The amount of odd oxygen directly removed is small ($NO_y \ll O_3$), and (ii) removal of NO_y suppresses O_3 production but does not produce
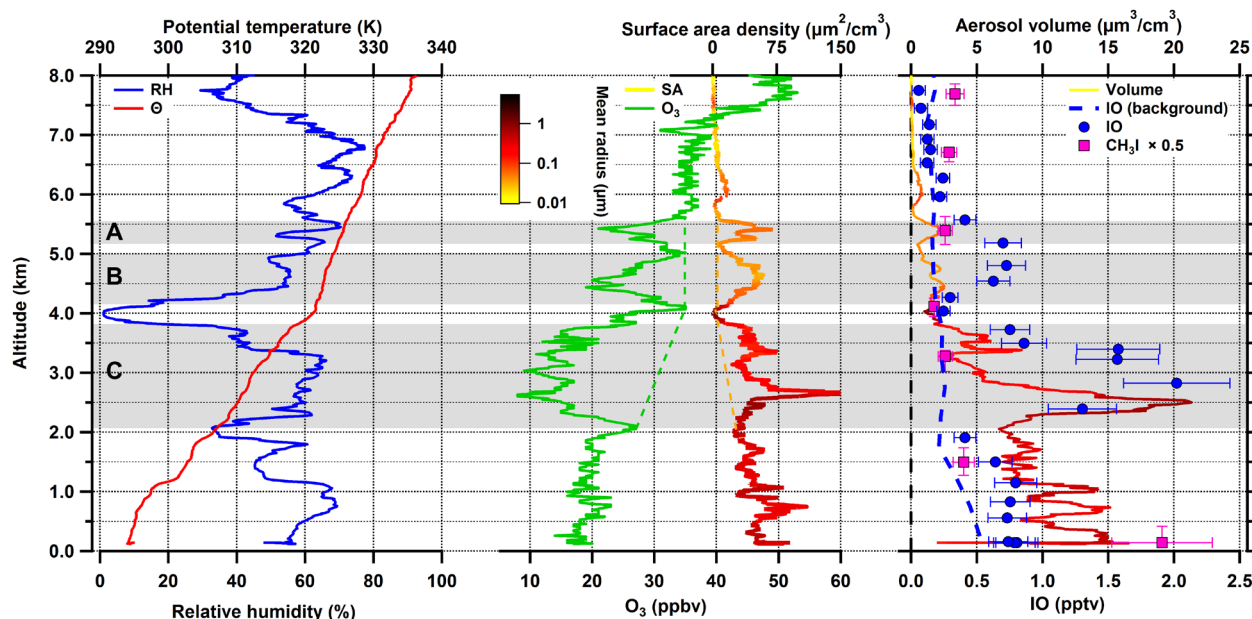
Fig. 2. Summary of RF05-01 case study. Left: Relative humidity and potential temperature. Middle: Demonstration of the anticorrelation of O_3 and aerosol surface area consistent with the literature and previously attributed to heterogeneous uptake. Gray shading across panels indicates when this smoothed surface area is greater than 25 $\mu m^2 cm^{-3}$; uppercase letters indicate the individual dust-layer intercepts. Dashed lines are indicative of a contiguous background. Right: Iodine observations; error bars show 1σ errors. Mixing ratios of IO are retrieved by the AMAX-DOAS using a parameterization method. Dashed line shows median of southern hemisphere TORERO observation after filtering for dust-impacted data. Aerosol volume density (box-car smoothed over 15 s for sufficient statistics) is shown. Water vapor was measured by the Vertical Cavity Surface-Emitting Laser (VCSEL) hygrometer. CH_3I is measured with Trace Organic Gas Analyzer (TOGA).

persistent chemical cycles to consume O_3. Even using theoretical maximal values for NO_y uptake ($\gamma = 1$), the impacts on ozone are the same (<0.1 ppb O_3 difference at all times). As a result, O_3 mixing ratios stabilize above 10 ppbv. Known heterogeneous reactions of O_3 and NO_y species are not enough to explain the observed low O_3 mixing ratios in the ozone-depleted laminae.

At the observed IO levels, gas-phase iodine chemistry is highly efficient at destroying additional O_3 through catalytic photochemical reaction cycles. Introducing 10 pptv of I_y (consistent with ~2 pptv of IO observed; fig. S4) accelerates O_3 destruction by over a factor of 2 and is needed to explain the low observed O_3 at the core of these layers. Only when the iodine is included can the box model explain the low O_3 below 10 ppbv (fig. S4). Iodine directly destroys O_3, dominates O_3 destruction as shown by the reaction integrals over 3 days (tables S4 and S5), and remains efficient even at these low O_3 concentrations. Critically, a distinct anticorrelation is observed: Iodine levels are highest where O_3 is lowest (fig. S5). Vigorous iodine chemistry consistent with known chemical mechanisms of gas-phase O_3 destruction by observed IO levels is needed and found to be sufficient to explain the ozone-depleted laminae.

It is possible that the multiphase reaction $I^- + O_3$ enhances the ozone sink beyond the gas-phase iodine chemistry modeled here. Any O_3 loss due to multiphase chemistry depends on the gas-phase O_3 concentration and on how the conditions sustaining I^- in aerosol change inside the dust layers relative to the background. Compared to the stratosphere (6), the contribution from $I^- + O_3$ in dust layers is masked by rapid gas-phase chemistry at much (factor ~ 150) higher gas-phase IO radical concentrations, lower O_3 concentrations (factor ~ 0.1), and the dilution of any dissolved iodide concentration in more abundant liquid water inside dust layers. Iodide in dust

aerosol is not enriched over background marine aerosol (36). Moreover, iodide would be depleted in less than 1 s if not replenished from other iodine reservoir species [e.g., iodate photoreduction (37, 38); see also the Supplementary Materials]. The photosensitized reduction of iodate in chromophoric dust proxies, while plausible as a source of I^- as an initial intermediate toward activating $I_{y,gas}$, is currently insufficiently constrained experimentally to model any accompanying multiphase O_3 loss with certainty. However, iodide destroys O_3 in a stoichiometric ratio of one, meaning that if 10 pptv $I_{y,gas}$ is liberated via $I^- + O_3$, this reaction consumes only 10 pptv of O_3. The direct O_3 sink of multiphase chemistry to liberate $I_{y,gas}$ is therefore very small compared to efficient gas-phase chemistry at the high observed IO radical concentrations, which destroys several ppbv of O_3. However, in the absence of a gas-phase mechanism to form HIO_3 (and thus particulate iodate), O_3 loss could be further enhanced and is estimated conservatively here. In the future, more measurements to understand iodine speciation and phase partitioning are needed to understand iodate as a missing component of the geochemical iodine cycle in models.

Aeolian iodine source from dust

While the large IO enhancements inside dust layers could, in principle, reflect a change in chemical partitioning of gas-phase iodine, we find that the dust itself is the source of the iodine. This is because, even under exceptionally low O_3 inside the dust layers, the IO/I_y ratio remains high, and IO accounts for at least 15% of daytime I_y. The photostationary equilibrium of gas-phase I_y reservoir species is limited by HOI photolysis and establishes within minutes (daytime). Therefore, changes in gas-phase chemical partitioning induced by dust are small, and to explain elevated IO inside dust

layers, an additional iodine source from the dust is needed. We posit that iodate reduction and volatilization is the source of iodine from dust.

We propose that the observed correlation of iodine with aerosol volume (fig. S5) results from sparingly soluble iodates on dust surfaces, which accumulate from atmospheric deposition and geogenic deposits (13, 39–41) before lofting. We suggest that acid deposition from the atmosphere onto dust, dust deliquescence, and possibly illumination may be critical steps facilitating iodine release from lofted dust (see Fig. 3 and below): the alkalinity of dust, scarcity of water, and limited illumination before lofting trap iodate. We attribute the sphericity of particles in the layers at high altitude and with increasing distance from the coast to dust deliquescence. This role of water vapor in the activation process is consistent with previous findings that water vapor correlates with the level of O_3 depletion associated with Saharan dust (42). Liquid water helps to mobilize sparingly soluble IO_3^- and also iron ions, which facilitates the photochemical production of peroxides either directly (43) or by using the iron ions (44). Iodate might then be reduced through reaction with the iron ions (45, 46), by H_2O_2 (47), by nitrite (48) photosensitized reactions (37, 38), or by numerous other species (49). Iodate reduction is thermodynamically favored over nitrate reduction and might serve to suppress renoxification. Acid uptake to lower pH, possibly aided by photosensitized reactions, may be necessary for iodate

reduction to proceed at an atmospherically relevant rate. At higher altitudes, dust has an important role as ice nuclei (50), and iodine, in turn, recycles on ice surfaces in the upper troposphere (Fig. 3) (5, 51, 52). Iodate has been previously observed on Saharan dust during several ship cruises and is notably depleted for the smallest dust aerosol sizes, which is consistent with surface area–dependent heterogeneous release (fig. S6) (36, 53). Iodate is present in Saharan dust [and caliche deposits below the Atacama; see (54, 55) and the Supplementary Materials] and is the likely source of iodine enhancements associated with dust that had previously been observed over the Atlantic (31, 32).

In contrast to the observations from the Saharan region, we do not observe any impact from dust on CH_3I (Fig. 2, right). This suggests that there is likely to be more than one mechanism of iodate reduction leading to possible variations in the speciation of volatile iodine released from dust. Laboratory studies of iodate reduction under conditions that resemble atmospheric aerosols are needed to develop missing mechanisms of iodate reduction in atmospheric models.

Atmospheric implications
The precise mechanism of iodine release from dust is currently unknown. However, we approximate the net effect of iodate processing (Fig. 3) in the CAM-chem model (8, 56) as an autocatalytic dust source, tuned to resemble observed dust-impacted IO concentrations in the
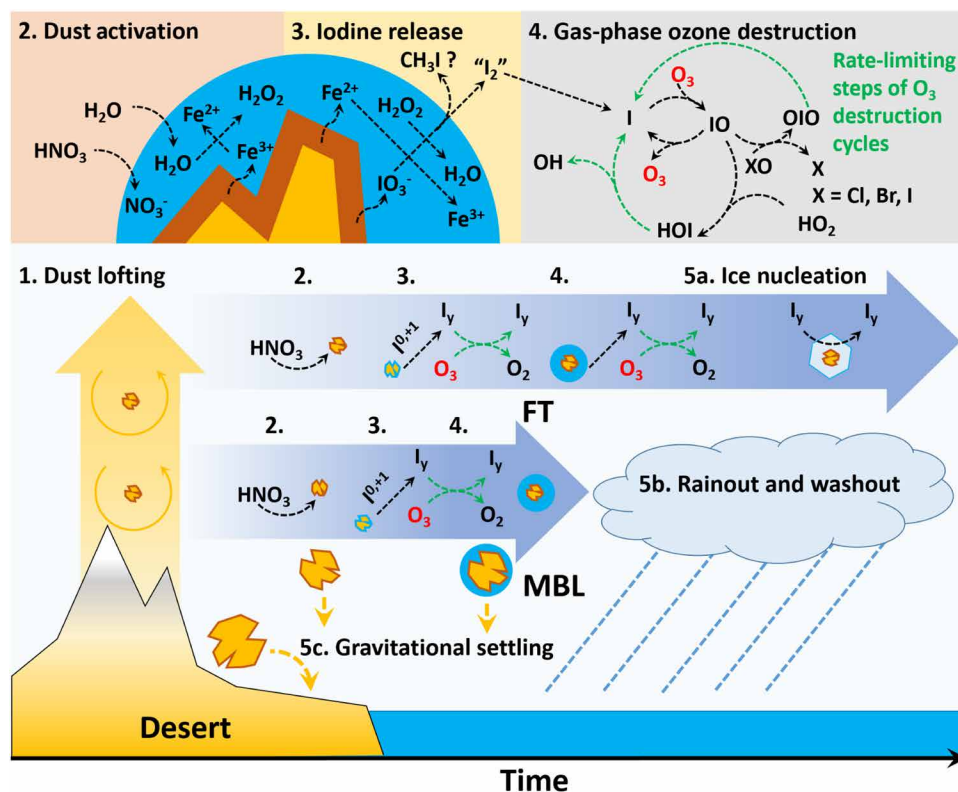

Fig. 3. Schematic of dust release of iodine and O_3 loss. Broadly clockwise from bottom left: (1) Aeolian processes loft dust, leading to size sorting due to gravitational settling. (2) The basicity of dust will encourage uptake of gas-phase acids such as nitric acid (HNO_3) and other NO_y species. (3) Once deliquesced aqueous ion chemistry is facilitated, iodate reduction can be facilitated by peroxides or soluble iron, either of which would suffice. The redox chemistry of iodine is highly complex, and the precise mechanism leading to volatilization is unknown. I_y is likely to be liberated in the oxidation state of I^0 (I_2) or I^+ (HOI, ICl, IBr) or as an organic species (e.g., CH_3I), although the latter is not observed in TORERO. (4) Released iodine photolyzes initiating rapid photochemical cycles. (5) Dust can participate in low-altitude cloud formation, is subject to wet deposition, and can nucleate ice, facilitating recycling of iodine on ice surfaces.

study area. The model captures the IO observed in the absence of dust, as well as the average IO enhancements in the presence of dust, yet it exhibits greater variability when dust is present (fig. S7). However, the latter may be expected given the limited number of observations. The spatial scale of the DOAS measurement is likely to include components of background air with lower IO. Nonetheless, IO enhancements of up to a factor of 10 over background were observed within the dust layers. The model underestimates the magnitude and variability of dust-free IO by a small amount in absolute terms, but this leads to a larger and more variable relative enhancement in dust-impacted data. The model has been tuned to capture the average IO concentrations measured in the presence of dust (fig. S7) within the studied region and is not affected by a similar difference in spatial scales. Hence, the median enhancements in fig. S7 are not directly comparable between model and observations, and the observations are expected to be a lower bound on the average IO enhancement inside dust layers. The model accurately produces the approximate vertical extent of the dust layers (Fig. 4B); an extended

horizontal domain is chosen to assess atmospheric impacts (allows the displacement of IO enhancements further from dust sources in the model; Fig. 4A). Dust is found to be the source of more than 90% of iodine outflow from the Atacama between 2- and 4-km height and dominates O_3 destruction in January (Fig. 4C).

Ozone impacts due to dust are conservatively estimated in the model and limited to iodine, because NO_y uptake to dust, as well as dust source of the Sechura Desert, is not represented in CAM-chem. The removal of NO_y (and by extension NO_x) will continue to suppress O_3 production until replenished, likely increasing its relevance at regional scales. The transport and chemistry of background O_3 levels are reasonably well represented (57–59). The model does not produce conditions similar to the O_3-depleted laminae aloft without introducing the new iodine source from dust, which suggests that transport of low O_3 air cannot explain the observed O_3 depletion in the dust laminae. As expected, modeled localized O_3 decreases by ~35% (Fig. 4D), which is less than observed. Nonetheless, a regional (box on Fig. 4, A and D) impact is clearly visible across most of the
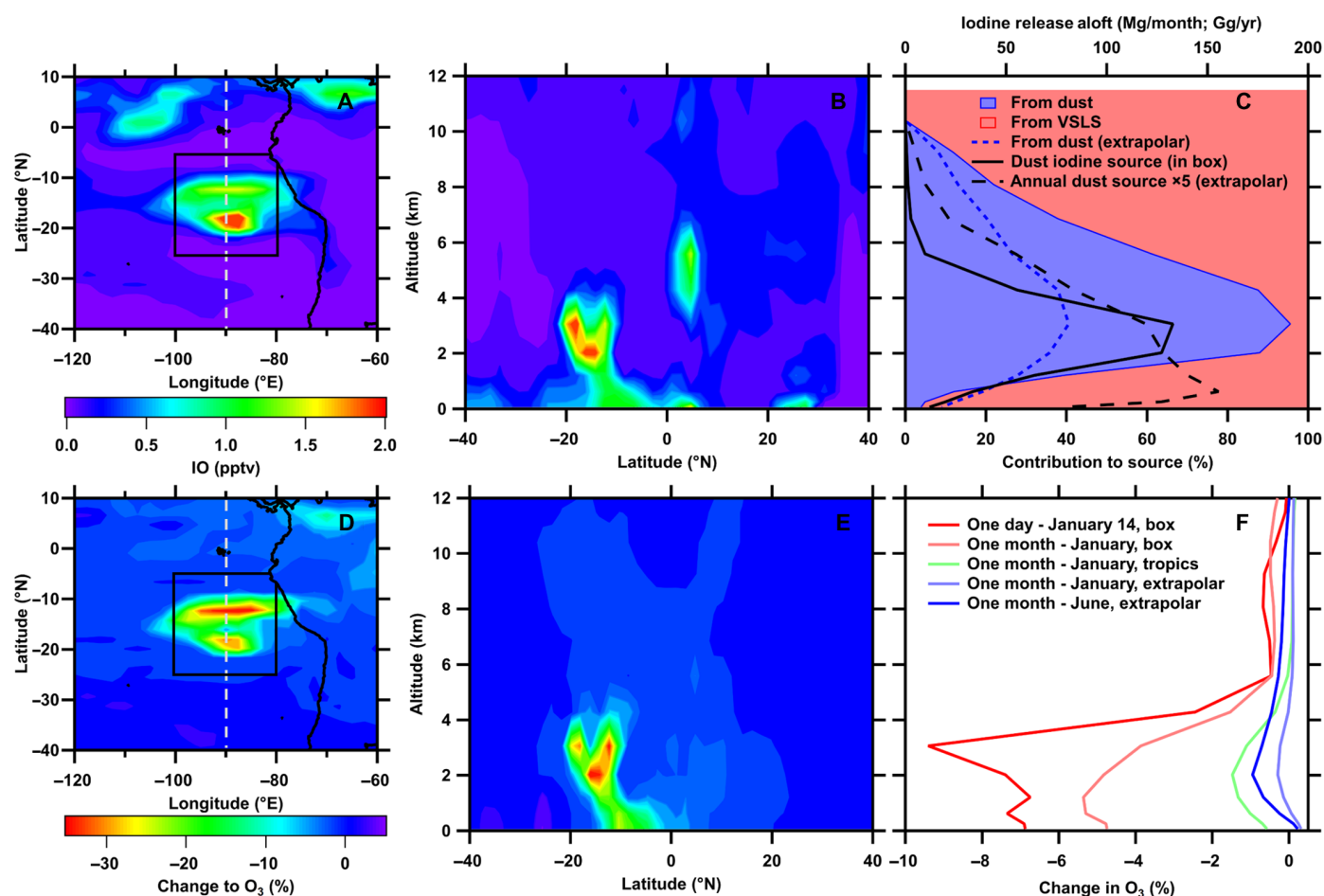

Fig. 4. Regional (and global) impacts. (**A**) Map of IO at 2.9-km altitude in CAM-chem for January 14 (dynamics in CAM-chem are fixed but do not reflect any specific real day). (**B**) Curtain of IO at 90°W (gray dashed line on map). (**C**) Iodine release at altitude and comparison of iodine release from dust and from very short lived species (VSLS) computed for January over the box indicated on the maps in Mg month^{-1} (top axis). Dashed lines show the same traces for an annual extrapolar average; fluxes are shown as Gg year^{-1} (top axis). (**D**) Impact of dust iodine on O_3 in CAM-chem computed as ($O_{3,dust\ iodine} - O_{3,base}$)/$O_{3,base}$. (**E**) Curtain of the O_3 impact at 90°W. (**F**) O_3 impacts at different temporal and spatial scales. The O_3 impact is computed by calculating the mean profiles for the two model cases and then computing the equation above. Displayed values are means computed for the box on the maps for January 14; the months of January and June; for the tropics (defined here as 20°S to 20°N) and for extrapolar regions (defined as 60°S to 60°N).

model domain, lowering O_3 by as much as −9.4% (−2.5 ppbv of O_3; Fig. 4F). In the free troposphere, iodine destroys O_3 150% as efficiently as in the MBL due to increased photolysis rates and has three to six times the residence time, greatly enhancing its impact (fig. S8). Downward transport entrains air into the MBL that is both enriched in iodine (Fig. 4B) and depleted in O_3 (Fig. 4E), leading to −6.9% (0.9 ppbv; regional) impact on O_3 at the surface and even −4.7% (−0.5 ppbv; regional) in the January mean. The entrainment of iodine-rich and O_3-depleted air into the MBL is of relevance to surface air quality and human health, and due to the iodine's buffer capacity over ozone, pollution is expected to evolve differently within regional scales in the near future depending on the air pollution mitigation policies implemented by different countries (57).

On a global scale, the Sahara dominates dust emissions, and the impacts of dust transport on surface air quality have been well documented in cities across Europe (60, 61). In our simulations, the iodine source from the Sahara is actively controlled and conservatively estimated by modulating the efficiency of iodine release zonally not to exceed the observed levels of IO radicals in the SAAD domain. Consistent with the SAAD dust, Saharan dust has also been observed to affect O_3 in the free troposphere at the Monte Cimone Climate observatory, with implications for surface air quality in cities of northern Italy [Po Valley; (28)] and southern Spain (62). This pattern of dust transport is captured by CAM-chem; however, the magnitude of episodic impacts on O_3 of >40% attributed to Saharan dust at Monte Cimone is underestimated in the model, reflecting the conservative implementation of iodine chemistry from Saharan dust (fig. S9). Transport and NO_y uptake are also likely to contribute substantially to O_3 depletion under more polluted conditions such as those observed at Monte Cimone (63). Similarly, dust from the Taklimakan and Gobi Deserts have been observed to affect O_3 in cities in northern China, although the impacts appear to be smaller (~10%) deep in the continental interior (29). While it is very likely that iodine impacts from dust are not limited to the study area, a confirmation of dust iodine release from other deserts globally, including the Sahara and Gobi Deserts, warrants further investigation. In our current conservative implementation, dust is found to be responsible for 41% of iodine release in the extrapolar lower free troposphere, resulting in an annual mean decrease of extrapolar tropospheric O_3 by 0.87%, which extends beyond the regional scale.

DISCUSSION

The persistence of IO radicals in aged stratospheric air further indicates that iodate heterogeneously recycles from stratospheric aerosols (6), which is consistent with our findings for dust. In the troposphere, particulate iodine is only a minor reservoir of total inorganic iodine (sum of gas- and particulate-phase I_y); most tropospheric iodine resides in the gas phase (8). The observations presented here suggest that iodate can be a primary source of iodine to the atmosphere. Together with the rapid oxidation and volatilization of iodide, this points to multiphase iodine chemistry being extremely dynamic and context dependent and warrants further research.

Surface deposits of iodine are the result of atmospheric deposition and geogenic iodate deposits in the Caliche layers of the Atacama Desert. Field measurements indicate that atmospheric HIO_3 is widespread (13) and available to deposit and accumulate on alkaline dust as iodate before lofting. In principle, also iodides, if present, can be oxidized to iodates in an oxic atmosphere (64). Iodate in the

subsurface Caliche layers is thought to be Jurassic marine deposits uplifted by the Andes orogeny, and slowly transported to their current location by ground water (55, 65, 66). Marine diagenesis is the major source of such geological iodine, given that the crustal budget of iodine is dominated by marine carbonates (67). Continental deposits of iodine are thus ultimately of marine origin (55) and can inject iodine to the atmosphere as part of volcanic eruptions (68, 69) and lofted dust. The relative importance of atmospheric deposition and geogenic iodine as sources of iodate injected to the atmosphere remains to be established.

The correlation of iodate with calcium (fig. S6; see the Supplementary Materials for details) suggests that iodate reduction could be important to consider in geoengineering scenarios, which have proposed annual stratospheric injections of calcium carbonate as large as 5.6 Tg year^{-1} (70). Iodate is a contaminant component of a variety of carbonate minerals (71), i.e., 1 to 10 parts per million (ppm) (72). Upper limits could lead to 3% year^{-1} increase in the current stratospheric iodine burden of 1.7 Gg (6). Over a decade, iodate injection as part of geoengineering dust injections thus has the potential to significantly increase the iodine burden in the lower stratosphere, which would slow ozone layer recovery.

Our results have broader implications for iodine partitioning between the gas and particle phases and add field evidence of iodate reduction as a missing component of the geochemical iodine cycle. Multiyear records show that iodine has increased by a factor of 3 since 1950, responding to O_3 anthropogenic pollution and thinning of polar sea ice (19–21). Atmospheric models are currently missing sources of iodic acid (HIO_3), which is a highly condensable vapor that adds iodate in particles and—as an alternative pathway to higher iodine oxides—can nucleate and grow particles efficiently (13). If atmospheric deposition of iodate is responsible for iodine accumulation on dust, it is currently unclear whether the released iodine we observe had accumulated before dust lofting on geological time scales or reflects the contemporary O_3 response of the oceanic iodine source enhancement. The iodine-mediated feedback between dust and tropospheric O_3 is likely to shift regional impacts relevant to air quality and human health in a changing climate. Predicting these changes in response to changing dust emissions on climate is challenging (73, 74) and deserves further attention. Investigation of the time scales of iodate cycling between the gas and particle phases, including deposition to arid regions and reemission as dust, is critical to quantifying the role of iodate and deserts as a missing piece in the global geochemical iodine cycle.

MATERIALS AND METHODS
The TORERO field campaign

The aircraft measurements were collected aboard the National Science Foundation (NSF)/National Center for Atmospheric Research (NCAR) High-performance Instrumented Airborne Platform for Environmental Research (HIAPER) GV aircraft during the Tropical Ocean tRoposphere Exchange of Reactive halogen species and Oxygenated volatile organic compounds (VOC) (TORERO) field campaign (5). TORERO conducted 17 research flights over the Eastern Pacific Ocean out of Antofagasta, Chile and San Jose, Costa Rica in January and February 2012. IO was measured with a CU AMAX-DOAS instrument (4, 5, 58) (see the Supplementary Materials). Aerosol backscatter and depolarization profiles were measured by the HSRL (75, 76) (see the Supplementary Materials). Submicrometer

particles were measured with an Ultra-High Sensitivity Aerosol Spectrometer (UHSAS) (77), and supermicrometer particles were measured with a Cloud Droplet Probe (CDP) (78). The up- and downwelling spectral actinic flux was measured by the HIAPER Airborne Radiation Package (HARP)—Actinic Flux (79) and used to compute photolysis frequencies. Organic iodine (particularly CH_3I) was measured with the NCAR Trace Organic Gas Analyzer (TOGA) (80, 81).

Identification and specification of dust layers
To ensure a consistent identification and definition of the dust layers and their extent, three criteria were used: (i) The aerosol surface area, when summed from the UHSAS and CDP assuming spherical particles, was greater than 25 to prevent extensive splitting of layers if the surface area drops below this threshold for less than 30 s, the layer is treated as contiguous; (ii) IO mixing ratios in the layer either are significantly greater than measured above or below the layer or are greater and at least 0.2 pptv when averaged; (iii) water and potential temperature profiles were examined to exclude the boundary layer. Using this definition, a total of 27 layers, ranging in altitude between 0.9 and 6.4 km, were identified during the TORERO campaign. All identified layers are from flights that landed or took off from Antofagasta, Chile. For a further classification of the layers and the naming convention, see the Supplementary Materials.

Back-trajectory data products
Two back-trajectory data products were used: (i) a 72-hour mesoscale product in the Weather Research and Forecasting (WRF) model (82) and (ii) a 10-day Real-time Air Quality Modeling System (RAQMS) product. The WRF back-trajectories were initialized along the flight track for ~2000 points per flight and ran back for 72 hours at 3-hour resolution with an advective time step of 30 min (83). The WRF simulations included a planetary boundary layer (PBL) tracer that was set to 1 within the model's PBL and allowed to spread above the PBL by various model processes. Surface source regions for a given trajectory were defined as the locations where the PBL tracer increased or the trajectory passed through the boundary layer. Boundary layer contributions were collected for 1° × 1° bins for every back trajectory ending in an iodine enhancement layer back 72 hours weighted by the amount of tracer increase (weight of 1 when in the boundary layer). Dust source regions are determined by selecting source areas with soil moisture below 0.075 cm^3 cm^{-3} at 1° × 1° resolution in the annual average based on the Soil Moisture Active Passive (SMAP) satellite (84). Reverse Domain Filling (85) in RAQMS chemical and meteorological forecasts (86) provides information on 10 days of air mass history for ~500 altitude curtains per flight along the flight track.

Chemical box modeling
$I_{y,gas}$ was inferred from IO radical measurements using a chemical box model developed at the University of Colorado Boulder (52, 58), with extended iodine chemistry (8) including photolysis frequencies measured with HARP—Actinic Flux (79) and chemical constraints from observations (see the Supplementary Materials for details). O_3 loss for different chemical scenarios was modeled using the same box model (table S3).

Global modeling
CAM-chem (version 4) (59) was used to estimate ozone loss and the iodine (I_y) budget. Model cases examining the recycling of iodine to the gas phase on different atmospheric surfaces are the same as in (6). The dust iodine source was represented as an extension of the iodine ($IONO_2$, INO_2, and HOI) recycling on sea-salt aerosol, although instead of just resulting in a change of I_y partitioning, the iodine recycling on dust surfaces produces an additional iodine source of 4% of the net heterogeneous recycling rate. The rate of this reaction was capped to saturate at 2 μm^2 cm^{-3} and further limited by latitude such that IO all over the globe never exceeds the maximum concentration observed during TORERO within the SAAD region (see the Supplementary Materials for details).

Statistical analysis
Unless otherwise specified, when referring to fitted correlations in the text, the input data are the specified quantities arithmetically averaged over layer intercepts, and orthogonal distance regression is used. Data are used without additional weighting, if data appear on a graph showing a correlation they were used in the fit. No composite or nonlinear fits are presented in this manner; hence, references to "R" or "R^2" refer to the Pearson product-moment correlation coefficient and the square thereof. Explicit hypothesis testing is not used.

REFERENCES AND NOTES
1. D. Smythe-Wright, S. M. Boswell, P. Breithaupt, R. D. Davidson, C. H. Dimmer, L. B. Eiras Diaz, Methyl iodide production in the ocean: Implications for climate change. *Global Biogeochem. Cycles* **20**, GB3003 (2006).
2. E. Suess, F. Aemisegger, J. E. Sonke, M. Sprenger, H. Wernli, L. H. E. Winkel, Marine versus continental sources of iodine and selenium in rainfall at two European high-altitude locations. *Environ. Sci. Technol.* **53**, 1905–1917 (2019).
3. B. Alicke, K. Hebestreit, J. Stutz, U. Platt, Iodine oxide in the marine boundary layer. *Nature* **397**, 572–573 (1999).
4. B. Dix, S. Baidar, J. F. Bresch, S. R. Hall, K. S. Schmidt, S. Wang, R. Volkamer, Detection of iodine monoxide in the tropical free troposphere. *Proc. Natl. Acad. Sci. U.S.A.* **110**, 2035–2040 (2013).
5. R. Volkamer, S. Baidar, T. L. Campos, S. Coburn, J. P. DiGangi, B. Dix, E. W. Eloranta, T. K. Koenig, B. Morley, I. Ortega, B. R. Pierce, M. Reeves, R. Sinreich, S. Wang, M. A. Zondlo, P. A. Romashkin, Aircraft measurements of BrO, IO, glyoxal, NO_2, H_2O, O_2–O_2 and aerosol extinction profiles in the tropics: Comparison with aircraft–/ship-based in situ and lidar measurements. *Atmos. Meas. Tech.* **8**, 2121–2148 (2015).
6. T. K. Koenig, S. Baidar, P. Campuzano-Jost, C. A. Cuevas, B. Dix, R. P. Fernandez, H. Guo, S. R. Hall, D. Kinnison, B. A. Nault, K. Ullmann, J. L. Jimenez, A. Saiz-Lopez, R. Volkamer, Quantitative detection of iodine in the stratosphere. *Proc. Natl. Acad. Sci. U.S.A.* **117**, 1860–1866 (2020).
7. K. A. Read, A. S. Mahajan, L. J. Carpenter, M. J. Evans, B. V. E. Faria, D. E. Heard, J. R. Hopkins, J. D. Lee, S. J. Moller, A. C. Lewis, L. Mendes, J. B. McQuaid, H. Oetjen, A. Saiz-Lopez, M. J. Pilling, J. M. C. Plane, Extensive halogen-mediated ozone destruction over the tropical Atlantic Ocean. *Nature* **453**, 1232–1235 (2008).
8. A. Saiz-Lopez, R. P. Fernandez, C. Ordóñez, D. E. Kinnison, J. C. Gómez Martín, J.-F. Lamarque, S. Tilmes, Iodine chemistry in the troposphere and its effect on ozone. *Atmos. Chem. Phys.* **14**, 13119–13143 (2014).
9. T. Sherwen, M. J. Evans, L. J. Carpenter, S. J. Andrews, R. T. Lidster, B. Dix, T. K. Koenig, R. Sinreich, I. Ortega, R. Volkamer, A. Saiz-Lopez, C. Prados-Roman, A. S. Mahajan, C. Ordóñez, Iodine's impact on tropospheric oxidants: A global model study in GEOS-Chem. *Atmos. Chem. Phys.* **16**, 1161–1186 (2016).
10. T. Sherwen, M. J. Evans, L. J. Carpenter, J. A. Schmidt, L. J. Mickley, Halogen chemistry reduces halogen-driven tropospheric O_3 radiative forcing. *Atmos. Chem. Phys.* **17**, 1557–1569 (2017).
11. A. Saiz-Lopez, J.-F. Lamarque, D. E. Kinnison, S. Tilmes, C. Ordóñez, J. J. Orlando, A. J. Conley, J. M. C. Plane, A. S. Mahajan, G. Sousa Santos, E. L. Atlas, D. R. Blake, S. P. Sander, S. Schauffler, A. M. Thompson, G. Brasseur, C. Ordóñez, J. J. Orlando, A. J. Conley, J. M. C. Plane, A. S. Mahajan, G. Sousa Santos, E. L. Atlas, D. R. Blake, S. P. Sander, S. Schauffler, A. M. Thompson, G. Brasseur, Estimating the climate significance of halogen-driven ozone loss in the tropical marine troposphere. *Atmos. Chem. Phys.* **12**, 3939–3949 (2012).

12. T. M. Sherwen, J. A. Schmidt, M. J. Evans, L. J. Carpenter, K. Großmann, S. D. Eastham, D. J. Jacob, B. Dix, T. K. Koenig, R. Sinreich, I. Ortega, R. Volkamer, A. Saiz-Lopez, C. Prados-Roman, A. S. Mahajan, C. Ordóñez, Global impacts of tropospheric halogens (Cl, Br, I) on oxidants and composition in GEOS-Chem. *Atmos. Chem. Phys.* **16**, 12239–12271 (2016).

13. X.-C. He, Y. J. Tham, L. Dada, M. Wang, H. Finkenzeller, D. Stolzenburg, S. Iyer, M. Simon, A. Kürten, J. Shen, B. Rörup, M. Rissanen, S. Schobesberger, R. Baalbaki, D. S. Wang, T. K. Koenig, T. Jokinen, N. Sarnela, L. J. Beck, J. Almeida, S. Amanatidis, A. Amorim, F. Ataei, A. Baccarini, B. Bertozzi, F. Bianchi, S. Brilke, L. Caudillo, D. Chen, R. Chiu, B. Chu, A. Dias, A. Ding, J. Dommen, J. Duplissy, I. El Haddad, L. Gonzalez Carracedo, M. Granzin, A. Hansel, A. Heinritzi, V. Hofbauer, H. Junninen, J. Kangasluoma, D. Kemppainen, C. Kim, W. Kong, J. E. Krechmer, A. Kvashin, T. Laitinen, H. Lamkaddam, C. P. Lee, K. Lehtipalo, M. Leiminger, Z. Li, V. Makhmutov, H. E. Manninen, G. Marie, R. Marten, S. Mathot, R. L. Mauldin, B. Mentler, O. Möhler, T. Müller, W. Nie, A. Onnela, T. Petäjä, J. Pfeifer, M. Philippov, A. Ranjithkumar, A. Saiz-Lopez, I. Salma, W. Scholz, S. Schuchmann, B. Schulze, G. Steiner, Y. Stozhkov, C. Tauber, A. Tomé, R. C. Thakur, O. Väisänen, M. Vazquez-Pufleau, A. C. Wagner, Y. Wang, S. K. Weber, P. M. Winkler, Y. Wu, M. Xiao, C. Yan, Q. Ye, A. Ylisirniö, M. Zauner-Wieczorek, Q. Zha, P. Zhou, R. C. Flagan, J. Curtius, U. Baltensperger, M. Kulmala, V.-M. Kerminen, T. Kurtén, N. M. Donahue, R. Volkamer, J. Kirkby, D. R. Worsnop, M. Sipilä, Role of iodine oxoacids in atmospheric aerosol nucleation. *Science* **371**, 589–595 (2021).

14. C. D. O'dowd, J. L. Jimenez, R. Bahreini, R. C. Flagan, J. H. Seinfeld, K. Hämeri, L. Pirjola, M. Kulmala, S. Gerard Jennings, T. Hoffmann, Marine aerosol formation from biogenic iodine emissions. *Nature* **417**, 632–636 (2002).

15. M. Sipilä, N. Sarnela, T. Jokinen, H. Henschel, H. Junninen, J. Kontkanen, S. Richters, J. Kangasluoma, A. Franchin, O. Peräkylä, M. P. Rissanen, M. Ehn, H. Vehkamäki, T. Kurten, T. Berndt, T. Petäjä, D. Worsnop, D. Ceburnis, V.-M. Kerminen, M. Kulmala, C. O'Dowd, Molecular-scale evidence of aerosol particle formation via sequential addition of HIO$_3$. *Nature* **537**, 532–534 (2016).

16. A. Baccarini, L. Karlsson, J. Dommen, P. Duplessis, J. Vüllers, I. M. Brooks, A. Saiz-Lopez, M. Salter, M. Tjernström, U. Baltensperger, P. Zieger, J. Schmale, Frequent new particle formation over the high Arctic pack ice by enhanced iodine emissions. *Nat. Commun.* **11**, 4924 (2020).

17. L. J. Carpenter, S. M. MacDonald, M. D. Shaw, R. Kumar, R. W. Saunders, R. Parthipan, J. Wilson, J. M. C. Plane, Atmospheric iodine levels influenced by sea surface emissions of inorganic iodine. *Nat. Geosci.* **6**, 108–111 (2013).

18. S. M. Macdonald, J. C. Gómez Martín, R. Chance, S. Warriner, A. Saiz-Lopez, L. J. Carpenter, J. M. C. Plane, A laboratory characterisation of inorganic iodine emissions from the sea surface: Dependence on oceanic variables and parameterisation for global modelling. *Atmos. Chem. Phys.* **14**, 5841–5852 (2014).

19. C. A. Cuevas, N. Maffezzoli, J. P. Corella, A. Spolaor, P. Vallelonga, H. A. Kjær, M. Simonsen, M. Winstrup, B. Vinther, C. Horvat, R. P. Fernandez, D. Kinnison, J.-F. Lamarque, C. Barbante, A. Saiz-Lopez, Rapid increase in atmospheric iodine levels in the North Atlantic since the mid-20th century. *Nat. Commun.* **9**, 1452 (2018).

20. M. Legrand, J. R. McConnell, S. Preunkert, M. Arienzo, N. Chellman, K. Gleason, T. Sherwen, M. J. Evans, L. J. Carpenter, Alpine ice evidence of a three-fold increase in atmospheric iodine deposition since 1950 in Europe due to increasing oceanic emissions. *Proc. Natl. Acad. Sci. U.S.A.* **115**, 12136–12141 (2018).

21. X. Zhao, X. Hou, W. Zhou, Atmospheric iodine (127I and 129I) record in spruce tree rings in the Northeast Qinghai-Tibet Plateau. *Environ. Sci. Technol.* **53**, 8706–8714 (2019).

22. N. Bell, L. Hsu, D. J. Jacob, M. G. Schultz, D. R. Blake, J. H. Butler, D. B. King, J. M. Lobert, E. Maier-Reimer, Methyl iodide: Atmospheric budget and use as a tracer of marine convection in global models. *J. Geophys. Res. Atmos.* **107**, ACH8-1–ACH8-12 (2002).

23. C. E. Jones, K. E. Hornsby, R. Sommariva, R. M. Dunk, R. von Glasow, G. McFiggans, L. J. Carpenter, Quantifying the contribution of marine organic gases to atmospheric iodine. *Geophys. Res. Lett.* **37**, L18804 (2010).

24. C. Ordóñez, J.-F. Lamarque, S. Tilmes, D. E. Kinnison, E. L. Atlas, D. R. Blake, G. Sousa Santos, G. Brasseur, A. Saiz-Lopez, Bromine and iodine chemistry in a global chemistry-climate model: Description and evaluation of very short-lived oceanic sources. *Atmos. Chem. Phys.* **12**, 1423–1447 (2012).

25. P. P. A. Smyth, R. Burns, R. J. Huang, T. Hoffman, K. Mullan, U. Graham, K. Seitz, U. Platt, C. O'Dowd, Does iodine gas released from seaweed contribute to dietary iodine intake? *Environ. Geochem. Health* **33**, 389–397 (2011).

26. B. C. Sive, R. K. Varner, H. Mao, D. R. Blake, O. W. Wingenter, R. Talbot, A large terrestrial source of methyl iodide. *Geophys. Res. Lett.* **34**, L17808 (2007).

27. M. de Reus, F. Dentener, A. Thomas, S. Borrmann, J. Ström, J. Lelieveld, Airborne observations of dust aerosol over the North Atlantic Ocean during ACE 2: Indications for heterogeneous ozone destruction. *J. Geophys. Res. Atmos.* **105**, 15263–15275 (2000).

28. P. Bonasoni, P. Cristofanelli, F. Calzolari, U. Bonafè, F. Evangelisti, A. Stohl, S. Zauli Sajani, R. van Dingenen, T. Colombo, Y. Balkanski, Aerosol-ozone correlations during dust transport episodes. *Atmos. Chem. Phys.* **4**, 1201–1215 (2004).

29. Y. Nan, Y. Wang, Observational evidence for direct uptake of ozone in China by Asian dust in springtime. *Atmos. Environ.* **186**, 45–55 (2018).

30. J. Lasne, M. N. Romanias, F. Thevenet, Ozone uptake by clay dusts under environmental conditions. *ACS Earth Sp. Chem.* **2**, 904–914 (2018).

31. J. Williams, V. Gros, E. Atlas, K. Maciejczyk, A. Batsaikhan, H. F. Schöler, C. Forster, B. Quack, N. Yassaa, R. Sander, R. Van Dingenen, Possible evidence for a connection between methyl iodide emissions and Saharan dust. *J. Geophys. Res. Atmos.* **112**, D07302 (2007).

32. O. Puentedura, M. Gil, A. Saiz-Lopez, T. Hay, M. Navarro-Comas, A. Gómez-Pelaez, E. Cuevas, J. Iglesias, L. Gomez, Iodine monoxide in the north subtropical free troposphere. *Atmos. Chem. Phys.* **12**, 4909–4921 (2012).

33. B. Dix, T. K. Koenig, R. Volkamer, Parameterization retrieval of trace gas volume mixing ratios from Airborne MAX-DOAS. *Atmos. Meas. Tech.* **9**, 5655–5675 (2016).

34. E. M. Abraham, M. D. Rodríguez, M. C. Rubio, L. Guida-Johnson, L. Gomez, C. Rubio, Disentangling the concept of "South American Arid Diagonal.". *J. Arid Environ.* **175**, 104089 (2020).

35. A. Lauterbach, in *Iodine Chemistry and Applications* (John Wiley & Sons Inc., 2014), pp. 213–220.

36. A. R. Baker, C. Yodle, Measurement report: Indirect evidence for the controlling influence of acidity on the speciation of iodine in Atlantic aerosols. *Atmos. Chem. Phys.* **21**, 13067–13076 (2021).

37. R. W. Saunders, R. Kumar, S. M. MacDonald, J. M. C. Plane, Insights into the photochemical transformation of iodine in aqueous systems: Humic acid photosensitized reduction of iodate. *Environ. Sci. Technol.* **46**, 11854–11861 (2012).

38. Ó. Gálvez, M. Teresa Baeza-Romero, M. Sanz, A. Saiz-Lopez, Photolysis of frozen iodate salts as a source of active iodine in the polar environment. *Atmos. Chem. Phys.* **16**, 12713 (2016).

39. B. S. Gilfedder, S. C. Lai, M. Petri, H. Biester, T. Hoffmann, Iodine speciation in rain, snow and aerosols. *Atmos. Chem. Phys.* **8**, 6069–6084 (2008).

40. S. C. Lai, T. Hoffmann, Z. Q. Xie, Iodine speciation in marine aerosols along a 30,000 km round-trip cruise path from Shanghai, China to Prydz Bay, Antarctica. *Geophys. Res. Lett.* **35**, L21803 (2008).

41. B. S. Gilfedder, R. Chance, U. Dettmann, S. C. Lai, A. R. Baker, Determination of total and non-water soluble iodine in atmospheric aerosols by thermal extraction and spectrometric detection (TESI). *Anal. Bioanal. Chem.* **398**, 519–526 (2010).

42. J. Andrey, E. Cuevas, M. C. Parrondo, S. Alonso-Pérez, A. Redondas, M. Gil-Ojeda, Quantification of ozone reductions within the Saharan air layer through a 13-year climatologic analysis of ozone profiles. *Atmos. Environ.* **84**, 28–34 (2014).

43. D. W. O'Sullivan, P. J. Neale, R. B. Coffin, T. J. Boyd, C. L. Osburn, Photochemical production of hydrogen peroxide and methylhydroperoxide in coastal waters. *Mar. Chem.* **97**, 14–33 (2005).

44. H. J. H. Fenton, Oxidation of tartaric acid in presence of iron. *J. Chem. Soc. Trans.* **65**, 899–910 (1893).

45. A. J. Fudge, K. W. Sykes, The reaction between ferric and iodide ions. Part I. Kinetics and mechanism. *J. Chem. Soc.* , 119–124 (1952).

46. P. Comba, M. Kerscher, T. Krause, H. F. Schöler, Iron-catalysed oxidation and halogenation of organic matter in nature. *Environ. Chem.* **12**, 381 (2015).

47. W. C. Bray, H. A. Liebhafsky, Reactions involving hydrogen peroxide, iodine and iodate ion. I. Introduction. *J. Am. Chem. Soc.* **53**, 38–44 (1931).

48. K. Kim, J. Ju, B. Kim, H. Y. Chung, L. Vetráková, D. Heger, A. Saiz-Lopez, W. Choi, J. Kim, Nitrite-induced activation of iodate into molecular iodine in frozen solution. *Environ. Sci. Technol.* **53**, 4892–4900 (2019).

49. P. L. Gentili, J. C. Micheau, Light and chemical oscillations: Review and perspectives. *J. Photochem. Photobiol. C Photochem. Rev.* **43**, 100321 (2020).

50. D. J. Cziczo, K. D. Froyd, Sampling the composition of cirrus ice residuals. *Atmos. Res.* **142**, 15–31 (2014).

51. A. Saiz-Lopez, S. Baidar, C. A. Cuevas, T. K. Koenig, R. P. Fernandez, B. Dix, D. E. Kinnison, J.-F. Lamarque, X. Rodriguez-Lloveras, T. L. Campos, R. Volkamer, Injection of iodine to the stratosphere. *Geophys. Res. Lett.* **42**, 6852–6859 (2015).

52. S. Wang, J. A. Schmidt, S. Baidar, S. Coburn, B. Dix, T. K. Koenig, E. Apel, D. Bowdalo, T. L. Campos, E. Eloranta, M. J. Evans, J. P. DiGangi, M. A. Zondlo, R.-S. Gao, J. A. Haggerty, S. R. Hall, R. S. Hornbrook, D. Jacob, B. Morley, B. Pierce, M. Reeves, P. Romashkin, A. ter Schure, R. Volkamer, Active and widespread halogen chemistry in the tropical and subtropical free troposphere. *Proc. Natl. Acad. Sci. U.S.A.* **112**, 9281–9286 (2015).

53. C. Yodle, thesis, University of East Anglia (2015).

54. G. E. Ericksen, "Geology and origin of the Chilean nitrate deposits" (Geological Survey Professional Paper 1188, U.S. Geological Survey, 1981); https://pubs.usgs.gov/pp/1188/report.pdf.

55. F. Álvarez, M. Reich, A. Pérez-Fodich, G. Snyder, Y. Muramatsu, G. Vargas, U. Fehn, Sources, sinks and long-term cycling of iodine in the hyperarid Atacama continental margin. *Geochim. Cosmochim. Acta* **161**, 50–70 (2015).

56. R. P. Fernandez, R. J. Salawitch, D. E. Kinnison, J.-F. Lamarque, A. Saiz-Lopez, Bromine partitioning in the tropical tropopause layer: Implications for stratospheric injection. *Atmos. Chem. Phys.* **14**, 13391–13410 (2014).

57. F. Iglesias-Suarez, A. Badia, R. P. Fernandez, C. A. Cuevas, D. E. Kinnison, S. Tilmes, J. F. Lamarque, M. C. Long, R. Hossaini, A. Saiz-Lopez, Natural halogens buffer tropospheric ozone in a changing climate. *Nat. Clim. Chang.* **10**, 147–154 (2020).

58. T. K. Koenig, R. Volkamer, S. Baidar, B. Dix, S. Wang, D. C. Anderson, R. J. Salawitch, P. A. Wales, C. A. Cuevas, R. P. Fernandez, A. Saiz-Lopez, M. J. Evans, T. Sherwen, D. J. Jacob, D. Schmidt, D. Kinnison, J.-F. Lamarque, E. C. Apel, J. C. Bresch, T. Campos, F. M. Flocke, S. R. Hall, S. B. Honomichl, R. Hornbrook, J. B. Jensen, R. Lueb, D. D. Montzka, L. L. Pan, J. M. Reeves, S. M. Schauffler, K. Ullmann, A. J. Weinheimer, E. L. Atlas, V. Donets, M. A. Navarro, D. Riemer, N. J. Blake, D. Chen, L. G. Huey, D. J. Tanner, T. F. Hanisco, G. M. Wolfe, BrO and Br$_y$ profiles over the Western Pacific: Relevance of inorganic bromine sources and a Br$_y$ minimum in the aged tropical tropopause layer. *Atmos. Chem. Phys.* **17**, 15245–15270 (2017).

59. J.-F. Lamarque, L. K. Emmons, P. G. Hess, D. E. Kinnison, S. Tilmes, F. Vitt, C. L. Heald, E. A. Holland, P. H. Lauritzen, J. Neu, J. J. Orlando, P. J. Rasch, G. K. Tyndall, CAM-chem: Description and evaluation of interactive atmospheric chemistry in the Community Earth System Model. *Geosci. Model Dev.* **5**, 369–411 (2012).

60. L. Perez, A. Tobias, X. Querol, N. Künzli, J. Pey, A. Alastuey, M. Viana, N. Valero, M. González-Cabré, J. Sunyer, Coarse particles from Saharan Dust and daily mortality. *Epidemiology* **19**, 800–807 (2008).

61. Q. Wang, J. Gu, X. Wang, The impact of Sahara dust on air quality and public health in European countries. *Atmos. Environ.* **241**, 117771 (2020).

62. R. Soler, J. F. Nicolás, S. Caballero, E. Yubero, J. Crespo, Depletion of tropospheric ozone associated with mineral dust outbreaks. *Environ. Sci. Pollut. Res.* **23**, 19376–19386 (2016).

63. S. E. Bauer, Y. Balkanski, M. Schulz, D. A. Hauglustaine, F. Dentener, Global modeling of heterogeneous chemistry on mineral aerosol surfaces: Influence on tropospheric ozone chemistry and comparison to observations. *J. Geophys. Res. Atmos.* **109**, 2304 (2004).

64. M. A. Brown, J. T. Newberg, M. J. Krisch, B. S. Mun, J. C. Hemminger, Reactive uptake of ozone on solid potassium iodide. *J. Phys. Chem. C* **112**, 5520–5525 (2008).

65. A. Pérez-Fodich, M. Reich, F. Álvarez, G. T. Snyder, R. Schoenberg, G. Vargas, Y. Muramatsu, U. Fehn, Climate change and tectonic uplift triggered the formation of the Atacama Desert's giant nitrate deposits. *Geology* **42**, 251–254 (2014).

66. F. Álvarez, M. Reich, G. Snyder, A. Pérez-Fodich, Y. Muramatsu, L. Daniele, U. Fehn, Iodine budget in surface waters from Atacama: Natural and anthropogenic iodine sources revealed by halogen geochemistry and iodine-129 isotopes. *Appl. Geochemistry* **68**, 53–63 (2016).

67. Y. Muramatsu, K. H. Wedepohl, The distribution of iodine in the earth's crust. *Chem. Geol.* **147**, 201–216 (1998).

68. A. Schönhardt, A. Richter, N. Theys, J. V. P. Burrows, Space-based observation of volcanic iodine monoxide. *Atmos. Chem. Phys.* **17**, 4857–4870 (2017).

69. H. Bureau, A. L. Auzende, M. Marocchi, C. Raepsaet, P. Munsch, D. Testemale, M. Mézouar, S. Kubsky, M. Carrière, A. Ricolleau, G. Fiquet, Modern and past volcanic degassing of iodine. *Geochim. Cosmochim. Acta* **173**, 114–125 (2016).

70. D. W. Keith, D. K. Weisenstein, J. A. Dykema, F. N. Keutsch, Stratospheric solar geoengineering without ozone loss. *Proc. Natl. Acad. Sci. U.S.A.* **113**, 14910–14914 (2016).

71. X. Feng, S. A. T. Redfern, Iodate in calcite, aragonite and vaterite CaCO$_3$: Insights from first-principles calculations and implications for the I/Ca geochemical proxy. *Geochim. Cosmochim. Acta* **236**, 351–360 (2018).

72. W. Lu, A. J. Dickson, E. Thomas, R. E. M. Rickaby, P. Chapman, Z. Lu, Refining the planktic foraminiferal I/Ca proxy: Results from the Southeast Atlantic Ocean. *Geochim. Cosmochim. Acta* **287**, 318–327 (2020).

73. A. T. Evan, C. Flamant, M. Gaetani, F. Guichard, The past, present and future of African dust. *Nature* **531**, 493–495 (2016).

74. J. F. Kok, D. S. Ward, N. M. Mahowald, A. T. Evan, Global and regional importance of the direct dust-climate feedback. *Nat. Commun.* **9**, 241 (2018).

75. S. T. Shipley, D. H. Tracy, E. W. Eloranta, J. T. Trauger, J. T. Sroga, F. L. Roesler, J. A. Weinman, High spectral resolution lidar to measure optical scattering properties of atmospheric aerosols 1: Theory and instrumentation. *Appl. Optics* **22**, 3716–3724 (1983).

76. P. Piironen, E. W. Eloranta, Demonstration of a high-spectral-resolution lidar based on an iodine absorption filter. *Opt. Lett.* **19**, 234 (1994).

77. Y. Cai, D. C. Montague, W. Mooiweer-Bryan, T. Deshler, Performance characteristics of the ultra high sensitivity aerosol spectrometer for particles between 55 and 800nm: Laboratory and field studies. *J. Aerosol Sci.* **39**, 759–769 (2008).

78. S. Lance, C. A. Brock, D. Rogers, J. A. Gordon, Water droplet calibration of the Cloud Droplet Probe (CDP) and in-flight performance in liquid, ice and mixed-phase clouds during ARCPAC. *Atmos. Meas. Tech.* **3**, 1683–1706 (2010).

79. R. E. Shetter, M. Müller, Photolysis frequency measurements using actinic flux spectroradiometry during the PEM-Tropics mission: Instrumentation description and some results. *J. Geophys. Res. Atmos.* **104**, 5647–5661 (1999).

80. E. C. Apel, A. J. Hills, R. Lueb, S. Zindel, S. Eisele, D. D. Riemer, A fast-GC/MS system to measure C$_2$ to C$_4$ carbonyls and methanol aboard aircraft. *J. Geophys. Res. Atmos.* **108**, 8794 (2003).

81. E. C. Apel, L. K. Emmons, T. Karl, F. Flocke, A. J. Hills, S. Madronich, J. Lee-Taylor, A. Fried, P. Weibring, J. Walega, D. Richter, X. Tie, L. Mauldin, T. Campos, A. Weinheimer, D. Knapp, B. Sive, L. Kleinman, S. Springston, R. Zaveri, J. Ortega, P. Voss, D. Blake, A. Baker, C. Warneke, D. Welsh-Bon, J. de Gouw, J. Zheng, R. Zhang, J. Rudolph, W. Junkermann, D. D. Riemer, Chemical evolution of volatile organic compounds in the outflow of the Mexico City Metropolitan area. *Atmos. Chem. Phys.* **10**, 2353–2375 (2010).

82. W. C. Skamarock, J. B. Klemp, J. Dudhia, D. O. Gill, D. Barker, M. G. Duda, X. Huang, W. Wang, J. G. Powers, "A description of the advanced research WRF version 3" (No. NCAR/TN-475+STR, University Corporation for Atmospheric Research, 2008); doi:10.5065/D68S4MVH.

83. M. T. Stoelinga, J. F. Bresch, P. A. Mooney, K. W. Manning, A users' guide to RIP Users 4.7: A program for visualizing mesoscale model output (2018); https://github.com/NCAR/RIP.

84. D. Entekhabi, S. Yueh, P. E. O'Neill, K. H. Kellogg, A. Allen, R. Bindlish, M. Brown, S. Chan, A. Colliander, W. T. Crow, N. Das, G. De Lannoy, R. S. Dunbar, W. N. Edelstein, J. K. Entin, V. Escobar, S. D. Goodman, T. J. Jackson, B. Jai, J. Johnson, E. Kim, S. Kim, J. Kimball, R. D. Koster, A. Leon, K. C. McDonald, M. Moghaddam, P. Mohammed, S. Moran, E. G. Njoku, J. R. Piepmeier, R. Reichle, F. Rogez, J. Shi, M. W. Spencer, S. W. Thurman, L. Tsang, J. Van Zyl, B. Weiss, R. West, *SMAP Handbook–Soil Moisture Active Passive: Mapping Soil Moisture and Freeze/Thaw from Space—KU Leuven* (JPL Publication, 2014);https://media.asf.alaska.edu/uploads/smap pdf/smap_handbook.pdf.

85. R. T. Sutton, H. Maclean, R. Swinbank, A. O'Neill, F. W. Taylor, High-resolution stratospheric tracer fields estimated from satellite observations using Lagrangian trajectory calculations. *J. Atmos. Sci.* **51**, 2995–3005 (1994).

86. T. D. Fairlie, M. A. Avery, R. B. Pierce, J. Al-Saadi, J. Dibb, G. Sachse, Impact of multiscale dynamical processes and mixing on the chemical composition of the upper troposphere and lower stratosphere during the Intercontinental Chemical Transport Experiment–North America. *J. Geophys. Res. Atmos.* **112**, D16S90 (2007).

87. R. B. Pierce, J. Schaack, J. A. Al-Saadi, T. D. Fairlie, C. Kittaka, G. Lingenfelser, M. Natarajan, J. Olson, A. Soja, T. Zapotocny, A. Lenzen, J. Stobie, D. Johnson, M. A. Avery, G. W. Sachse, A. Thompson, R. Cohen, J. E. Dibb, J. Crawford, D. Rault, R. Martin, J. Szykman, J. Fishman, Chemical data assimilation estimates of continental U.S. ozone and nitrogen budgets during the Intercontinental Chemical Transport Experiment–North America. *J. Geophys. Res. Atmos.* **112**, 12–21 (2007).

88. D. Müller, A. Ansmann, I. Mattis, M. Tesche, U. Wandinger, D. Althausen, G. Pisani, Aerosol-type-dependent lidar ratios observed with Raman lidar. *J. Geophys. Res. Atmos.* **112**, D16202 (2007).

89. V. Noel, H. Chepfer, G. Ledanois, A. Delaval, P. H. Flamant, Classification of particle effective shape ratios in cirrus clouds based on the lidar depolarization ratio. *Appl. Optics* **41**, 4245–4257 (2002).

90. T. Sakai, T. Nagai, Y. Zaizen, Y. Mano, Backscattering linear depolarization ratio measurements of mineral, sea-salt, and ammonium sulfate particles simulated in a laboratory chamber. *Appl. Optics* **49**, 4441–4449 (2010).

91. N. Sugimoto, C. H. Lee, Characteristics of dust aerosols inferred from lidar depolarization measurements at two wavelengths. *Appl. Optics* **45**, 7468–7474 (2006).

92. W.-N. Chen, S.-Y. Chang, C. C.-K. Chou, Y.-W. Chen, J.-P. Chen, Study of relationship between water-soluble Ca^{2+} and lidar depolarization ratio for spring aerosol in the boundary layer. *Atmos. Environ.* **41**, 1440–1455 (2007).

93. M. Tesche, A. Ansmann, D. Müller, D. Althausen, R. Engelmann, V. Freudenthaler, S. Groß, Vertically resolved separation of dust and smoke over Cape Verde using multiwavelength Raman and polarization lidars during Saharan Mineral Dust Experiment 2008. *J. Geophys. Res. Atmos.* **114**, D13202 (2009).

94. B. van Diedenhoven, A. M. Fridlind, A. S. Ackerman, B. Van Diedenhoven, A. M. Fridlind, A. S. Ackerman, Influence of humidified aerosol on Lidar depolarization measurements below ice-precipitating Arctic Stratus. *J. Appl. Meteorol. Climatol.* **50**, 2184–2192 (2011).

95. D. P. Donovan, H. Klein Baltink, J. S. Henzing, S. R. de Roode, A. P. Siebesma, A depolarisation lidar-based method for the determination of liquid-cloud microphysical properties. *Atmos. Meas. Tech.* **8**, 237–266 (2015).

96. L. Guo, W. Gu, C. Peng, W. Wang, Y. Jie Li, T. Zong, Y. Tang, Z. Wu, Q. Lin, M. Ge, G. Zhang, M. Hu, X. Bi, X. Wang, M. Tang, A comprehensive study of hygroscopic properties of calcium-and magnesium-containing salts: Implication for hygroscopicity of mineral dust and sea salt aerosols. *Atmos. Chem. Phys.* **19**, 2115–2133 (2019).

97. U. Platt, J. Stutz, *Differential Optical Absorption Spectroscopy—Principles and Applications* (Springer, 2008).

98. T. Danckaert, C. Fayt, M. van Roozendael, I. de Smedt, V. Letocart, A. Merlaud, G. Pinardi, QDOAS software user manual v2.1 (2012); http://uv-vis.aeronomie.be/software/QDOAS/QDOAS_manual.pdf.

99. T. Deutschmann, S. Beirle, U. Frieß, M. Grzegorski, C. Kern, L. Kritten, U. Platt, C. Prados-Román, J. Puķīte, T. Wagner, B. Werner, K. Pfeilsticker, The Monte Carlo atmospheric radiative

transfer model McArtim: Introduction and validation of Jacobians and 3D features. *J. Quant. Spectrosc. Radiat. Transf.* **112**, 1119–1137 (2011).

100. H. Chen, C. O. Stanier, M. A. Young, V. H. Grassian, A kinetic study of ozone decomposition on illuminated oxide surfaces. *J. Phys. Chem. A* **115**, 11979–11987 (2011).

101. A. Vlasenko, T. Huthwelker, H. W. Gäggeler, M. Ammann, Kinetics of the heterogeneous reaction of nitric acid with mineral dust particles: An aerosol flowtube study. *Phys. Chem. Chem. Phys.* **11**, 7921–7930 (2009).

102. M. Tang, X. Huang, K. Lu, M. Ge, Y. Li, P. Cheng, T. Zhu, A. Ding, Y. Zhang, S. Gligorovski, W. Song, X. Ding, X. Bi, X. Wang, Heterogeneous reactions of mineral dust aerosol: Implications for tropospheric oxidation capacity. *Atmos. Chem. Phys.* **17**, 11727–11777 (2017).

103. W. L. Chameides, The photochemistry of a remote marine stratiform cloud. *J. Geophys. Res.* **89**, 4739 (1984).

104. M. Ammann, R. A. Cox, J. N. Crowley, M. E. Jenkin, A. Mellouki, M. J. Rossi, J. Troe, T. J. Wallington, Evaluated kinetic and photochemical data for atmospheric chemistry: Volume VI—Heterogeneous reactions with liquid substrates. *Atmos. Chem. Phys.* **13**, 8045–8228 (2013).

105. N. W. Oldridge, J. P. D. Abbatt, Formation of gas-phase bromine from interaction of ozone with frozen and liquid NaCl/NaBr solutions: Quantitative separation of surficial chemistry from bulk-phase reaction. *J. Phys. Chem. A* **115**, 2590–2598 (2011).

106. L. Magi, F. Schweitzer, C. Pallares, S. Cherif, P. Mirabel, C. George, Investigation of the uptake rate of ozone and methyl hydroperoxide by water surfaces. *J. Phys. Chem. A* **101**, 4943–4949 (1997).

107. J. J. Pueyo, G. Chong, M. Vega, Mineralogy and parental brine evolution in the Pedro de Valdivia nitrate deposit, Antofagasta, Chile. *Andean Geol.* **25**, 3–15 (2010).

108. D. E. Polyak, *2012 Minerals Yearbook* (U.S. Geological Survey, 2016); https://s3-us-west-2. amazonaws.com/prd-wret/assets/palladium/production/mineral-pubs/iodine/ myb1-2012-iodin.pdf.

109. J. A. Rutllant, R. C. Muñoz, R. D. Garreaud, Meteorological observations on the northern Chilean coast during VOCALS-REx. *Atmos. Chem. Phys.* **13**, 3409–3422 (2013).

110. F. Keppler, R. Eiden, V. Niedan, J. Pracht, H. F. Schöler, Halocarbons produced by natural oxidation processes during degradation of organic matter. *Nature* **403**, 298–301 (2000).

111. K. Kandler, N. Benker, U. Bundke, E. Cuevas, M. Ebert, P. Knippertz, S. Rodríguez, L. Schütz, S. Weinbruch, Chemical composition and complex refractive index of Saharan Mineral Dust at Izaña, Tenerife (Spain) derived by electron microscopy. *Atmos. Environ.* **41**, 8058–8074 (2007).

112. I. Barikmo, S. Henjum, L. Dahl, A. Oshaug, L. E. Torheim, Environmental implication of iodine in water, milk and other foods used in Saharawi refugees camps in Tindouf, Algeria. *J. Food Compos. Anal.* **24**, 637–641 (2011).

113. K. Oldenburg, A. Vogler, I. Mikó, O. Horváth, Photoredox decomposition of tin(II), lead(II), antimony(III) and bismuth(III) iodide complexes in solution. *Inorganica Chim. Acta* **248**, 107–110 (1996).

114. M. A. Brown, P. D. Ashby, D. F. Ogletree, M. Salmeron, J. C. Hemminger, Reactivity of ozone with solid potassium iodide investigated by atomic force microscopy. *J. Phys. Chem. C* **112**, 8110–8113 (2008).

115. P. Spietz, J. C. Gómez Martín, J. P. Burrows, Spectroscopic studies of the I_2/O_3 photochemistry: Part 2. Improved spectra of iodine oxides and analysis of the IO absorption spectrum. *J. Photochem. Photobiol. A Chem.* **176**, 50–67 (2005).

116. L. S. Rothman, I. E. Gordon, R. J. Barber, H. Dothe, R. R. Gamache, A. Goldman, V. I. Perevalov, S. A. Tashkun, J. Tennyson, HITEMP, the high-temperature molecular spectroscopic database. *J. Quant. Spectrosc. Radiat. Transf.* **111**, 2139–2150 (2010).

117. A. C. Vandaele, C. Hermans, P. C. Simon, M. Carleer, R. Colin, S. Fally, M. F. Mérienne, A. Jenouvrier, B. Coquart, Measurements of the NO_2 absorption cross-section from 42 000 cm^{-1} to 10 000 cm^{-1} (238–1000 nm) at 220 K and 294 K. *J. Quant. Spectrosc. Radiat. Transf.* **59**, 171–184 (1998).

118. K. Bogumil, J. Orphal, T. Homann, S. Voigt, P. Spietz, O. C. Fleischmann, A. Vogel, M. Hartmann, H. Kromminga, H. Bovensmann, J. Frerick, J. P. Burrows, Measurements of molecular absorption spectra with the SCIAMACHY pre-flight model: Instrument characterization and reference data for atmospheric remote-sensing in the 230–2380 nm region. *J. Photochem. Photobiol. A Chem.* **157**, 167–184 (2003).

119. R. Thalman, R. Volkamer, Temperature dependent absorption cross-sections of O_2-O_2 collision pairs between 340 and 630 nm and at atmospherically relevant pressure. *Phys. Chem. Chem. Phys.* **15**, 15371–15381 (2013).

120. S. Kraus, thesis, University of Mannheim (2006).

121. A. O. Langford, R. Schofield, J. S. Daniel, R. W. Portmann, M. L. Melamed, H. L. Miller, E. G. Dutton, S. Solomon, On the variability of the Ring effect in the near ultraviolet: Understanding the role of aerosols and multiple scattering. *Atmos. Chem. Phys.* **7**, 575–586 (2007).

122. R. Volkamer, P. Spietz, J. Burrows, U. Platt, High-resolution absorption cross-section of glyoxal in the UV-vis and IR spectral ranges. *J. Photochem. Photobiol. A Chem.* **172**, 35–46 (2005).

Science Advances

Ozone depletion due to dust release of iodine in the free troposphere

Theodore K. KoenigRainer VolkamerEric C. ApelJames F. BreschCarlos A. CuevasBarbara DixEdwin W. ElorantaRafael
P. FernandezSamuel R. HallRebecca S. HornbrookR. Bradley PierceJ. Michael ReevesAlfonso Saiz-LopezKirk Ullmann

View the article online
https://www.science.org/doi/10.1126/sciadv.abj6544
Permissions
https://www.science.org/help/reprints-and-permissions

Use of think article is subject to the Terms of service